JOURNAL OF APPLIED ELECTROCHEMISTRY 22 (1992) 668–674

Scale-up studies of an Fe/Cr redox flow battery based on shunt current analysis

G. CODINA, A. ALDAZ

Departamento de Química-Física, Universidad de Alicante, Aptdo. 99, E-03080 Alicante, Spain

Received 1 September 1991; revised 20 November 1991

Scale-up studies of a 0.7 kW single stack redox flow battery to a 2.1 kW three-stack assembly based on shunt current analysis are presented. The influence of the shunt-dependant design parameters on the energy efficiency of the system has been analysed for a single stack battery. Scale-up studies have been carried out in order to achieve energy efficiency in the three-stack assembly similar to that obtained for the single-stack system. The influence of the length of the hydraulic interconnection of the stacks and the assembly current on energy efficiency has been analysed. A shunt current calculation model for a three-stack assembly has been developed.

1. Introduction

It is well known that the transmission of electrical power by high voltage/low current devices is more efficient than by low voltage/high current transmission. Thus, bipolar stacks are used in electrochemical electrical power storage systems [1]. Likewise, in large electrosynthesis processes [2], this better energy efficiency of bipolar assemblies is an important factor in process design. In bipolar assemblies, the stack has a parallel flow distribution and the reactants are fed and collected by manifolds.

These reactant-filled pipes make up a secondary resistor network. The existence of a voltage gradient inside each cell produces an ionic shunt current through these conductive paths. Thus, in batteries in charge or in electrolytic cells, a fraction of the energy supplied to the system is shunted through the electrolyte network and is not used in the electrolytic process. In the same way, fuel cells and batteries in discharge also suffer a loss in energy efficiency due to shunt currents. The shunt currents are located in the electrode zones near the electrolyte ports and the electrochemical reactions carried out by these currents may take place at very high current densities.

These reactions can affect electrodes, reagents and the supporting electrolyte producing electrode corrosion and even disintegration. Undesirable gas evolution may also arise from the supporting electrolyte or solvent electrolysis. These reactions produce loss in energy efficiency, component wear, security problems and non-uniform current and voltage distribution. Moreover, if metallic deposition processes are involved, this non-uniformity in voltage and current distribution causes dendritic growth which may produce a short-circuit between two cells. This can be very dangerous when the electrochemical system to be treated is a battery due to the decrease of the output voltage in discharge.

In the literature, several solutions for diminishing shunt currents have been proposed. These solutions usually include increase of the path length of the electrolyte and decrease of its cross section. However, the increase in the electrical resistance of the electrolyte path implies an increasing loss in pumping power [3–5]. Therefore, the influence of the dimensions of manifolds and feeding ports on shunt currents is important in system design. The use of a multiple-stack assembly against a single stack containing the same number of cells presents some advantages in order to minimize parasitic losses of energy due to pumping power.

Voltage efficiency is defined as the ratio between the voltage of the battery in discharge and charge operations at a fixed state of charge. This state of charge has been fixed at 50% in agreement with the results reported in the literature [3, 16]. Current efficiency is defined as the ratio between the charge returned and introduced in the system between two fixed states of charge. Energy efficiency is defined as the ratio between the energy returned and introduced in the system between two fixed states of charge. This last parameter can be calculated approximately by multiplying the voltage and current efficiencies.

The aim of this paper is the analysis of the shunt-dependant parameters of an Fe/Cr redox flow battery formed by an assembly of three-stacks of filter press cells. The analysis was two-fold. First, an analysis and selection of the design parameters for a single-stack battery was made. Once these parameters were optimized, the battery was scaled-up to a three-stack assembly and the new characteristic design parameters of this kind of assembly, the hydraulic interconnection length and the total current, were also analysed.

The criterion used for analysis was a more energy efficiency than 70% using ports and manifold cross-sections as large as possible in order to diminish parasitic losses due to pumping. These energetic losses due to electrolyte pumping have not been considered in an explicit form in our optimization model due to the low

0021-891X/92

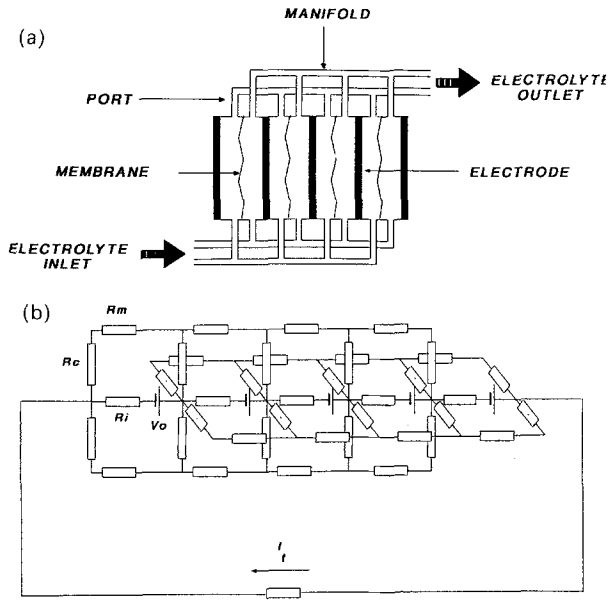

Fig. 1. (a) Schematic of a redox flow cell single-stack assembly. (b) Circuit analog.

pressure drops presented in the prototypes built at this laboratory. Moreover, the high concentration of our electrolytes allows low electrolyte flows to be used. Analysis of shunt currents have been made by several authors by applying Kirchoff's laws to electrical circuit analogs of the stacks of cells.

Most investigators use linear elements (resistors and d.c. voltage sources) [14, 17–23]. However, Katz [24] and Kuhn *et al.* [25] incorporate Zener diodes with different polarization curves. The Zener diode response is a good approximation to electrode polarization processes. The effect of conducting manifolds on shunt currents and system performance has also been studied by Burney *et al.* [26]. Recently, Szpak *et al.* [27] have proposed a model to evaluate shunt currents of bipolar stacks electrically connected in parallel.

From the results reported by these workers, it must be pointed out that manifold currents flow in the opposite direction to the cell current when the battery is in charge and in the same direction when the battery is in discharge. Thus, cell currents during charge are smaller than total current and cell currents during discharge are larger. Both facts produce a non-uniform voltage distribution in the cells of the stack. Cell voltage reaches a minimum at the central cell of the stack. Shunt currents in bipolar stacks electrically connected in series with parallel feeding have not been treated yet.

In this paper, a model to evaluate shunt currents in an assembly formed by three bipolar stacks with parallel electrolyte feeding is proposed.

2. Models

2.1. *Single stack model*

In Fig. 1, a diagram of a single-stack redox flow cell assembly (a) and its analog circuit (b) is shown. In this model, the following assumptions have been made:

(i) Electrolyte frames and pipes are made from a non-conducting material and the electrolyte-filled pipes are represented by a resistor, resistors placed in equivalent places being identical.
(ii) Electrodes have zero specific resistivity.
(iii) Cells are represented by an ideal d.c. voltage source (no electrode polarization processes are involved) and the internal cell resistance is represented by a resistor, resistors placed at equivalent places being identical.
(iv) Energy losses due to reactant cross-diffusion through the membrane are neglected.
(v) No competitive reactions are considered.

The various components are represented as follows: R_i, internal cell resistance; V_o, open-circuit cell voltage; R_c, port feed and exit resistance; R_m, manifold segment resistance; and I_t, charge–discharge current. Each cell, except the two terminal ones, generates four independent current loops, these loops having their own cell as a common element. Terminal cells only generate two current loops due to the fact that the electrolyte network is interrupted in the pumping section.

Therefore, the circuit described above is defined by a set of 4N–4 loop currents that must satisfy the same number of Kirchoff equations (1):

$$\sum_{j}^{p} i_j R_j - V_o = 0 \qquad (1)$$

where p is the number of resistors in each loop. Real currents i_j can be calculated as a function of loop currents I_k using Equation 2:

$$i_j = \sum_{k}^{q} I_k \qquad (2)$$

where q is the number of loop currents in each circuit branch.

The value of each equivalent resistor R_j may be calculated using Equation 3:

$$R_i = \rho L_i / A_i \qquad (3)$$

where ρ is the specific resistivity of the electrolyte, L is the pipe length and A is the pipe cross-sectional area.

Shunt current has been defined as the difference between total current I_t and the effective current circulating through each cell. A more detailed description of the system of equations generated and its resolution may be found in the literature cited [22].

2.2. *Three-stack model*

The diagram of a battery formed by three stacks connected in series with parallel electrolyte flow distribution (a) and its analog circuit (b) are shown in Fig. 2. The same assumptions used in the preceding model have been made. However, in order to minimize the number of equations to be solved, a new approximation has been made. This approximation consists in the treatment of each stack as composed by undivided cells. Thus, the value of the new resistor R_m (manifold

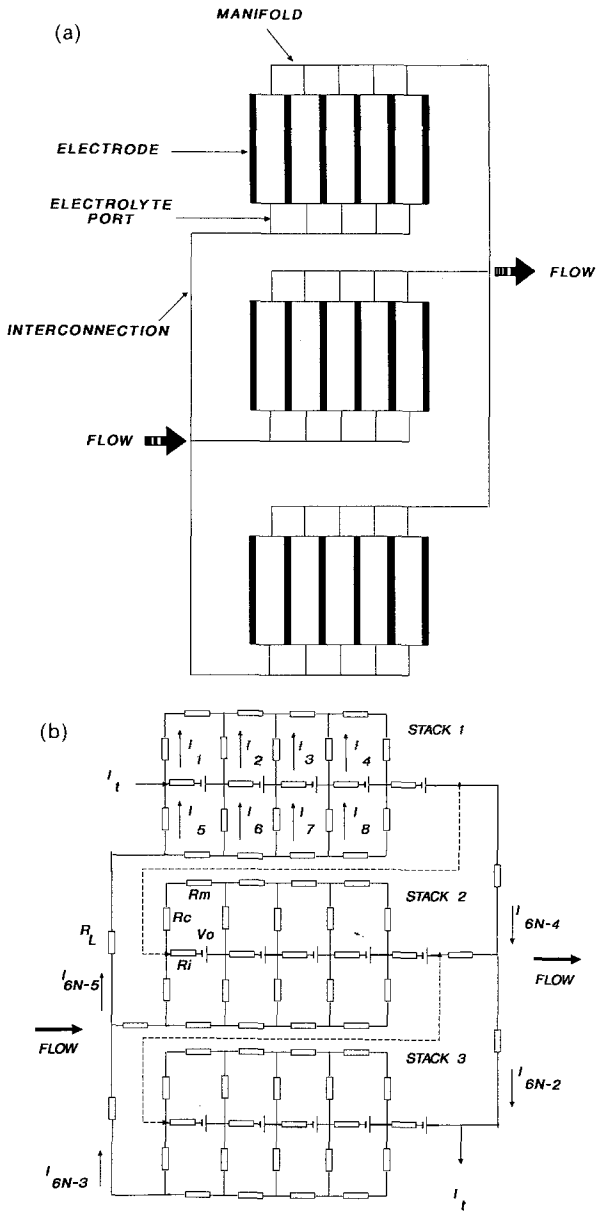

Fig. 2. (a) Schematic of a redox flow cell three-stack assembly. (b) Circuit analog.

resistance) is assumed to be the equivalent resistor of a parallel coupling of two R_m values calculated for the two different electrolytes flowing inside the cell. The value of the new resistor R_c may be calculated in an equivalent way. A suitable performance of this assumption has previously been tested by White *et al.* [22].

The components of the system have been represented in the same way as in the preceding model. The new element introduced, R_L, represents the resistor corresponding to the hydraulic interconnection of the stacks (Fig. 2). The electric circuit generated is defined by a set of 6N–2 Kirchoff equations (Equations 1 and 2). The value of each resistor can be calculated using Equation 3.

The mathematical resolution of this equation system was carried out using the software developed in our laboratory based upon the simple iteration method [28]. The results obtained for the single-stack battery were compared with that obtained using the same input parameters as in the literature [22]. Total agreement between these two calculations was obtained.

Table 1. Nominal design specifications for the single-stack redox flow battery

Nominal power	0.7 kW
Gross power	1.6 kW
Voltage (o.c., 50% state of charge)	18.6 V
Number of stacks	1
Number of cells per stack	18
Cell active area	1000 cm^2
Nominal current density	40 mA cm^{-2}
Cell resistivity	3 Ω cm^2
Equivalent resistors	
Port	221 Ω
Manifold	1.73 Ω

3. Results and discussion

3.1. *Single-stack assembly analysis*

The design parameters of a 0.7 kW single-stack Fe/Cr battery are presented in Table 1. The parameters analysed were the number of cells, current, manifold and port cross-section.

3.1.1. Number of cells. The number of cells forming a bipolar stack is an important design parameter due to the fact that it determines the voltage of the resulting stack. In Fig. 3a the shunt current in the central cell of the stack is shown as a function of the number of cells. A notable increase of the shunt current with the number of cells is observed. The values obtained in charge are larger than in discharge due to the fact that the cell voltage in charge is also larger. The difference between these two values is larger when the number of cells is increased because the difference between the charge and discharge voltages also increase.

In Fig. 3b the overall efficiencies of the stack as a function of the number of cells are represented. Voltage efficiency showed no significant variations when the number of cells was increased because, in this case, internal cell resistance is the predominant factor. This result is due to the low voltage drops produced by internal cell resistance compared with the open-circuit cell voltage.

Logically, current efficiency diminishes with the number of cells as a consequence of the increase of the shunt currents. As voltage efficiency stays constant in the range studied, the variation of energy efficiency as a function of the number of cells is similar to that presented by current efficiency.

From these results, it can be concluded that working with stacks formed by 18–20 cells, energy efficiencies higher than 77% may be expected. If power demand was greater, the designed stack could be incremented to 40 cells, maintaining over 75% energy efficiency.

3.1.2. Charge-discharge current. Current density and the number of cells are the parameters which must satisfy the power requirements of the system. In Fig. 4a shunt current at the central cell of the stack is

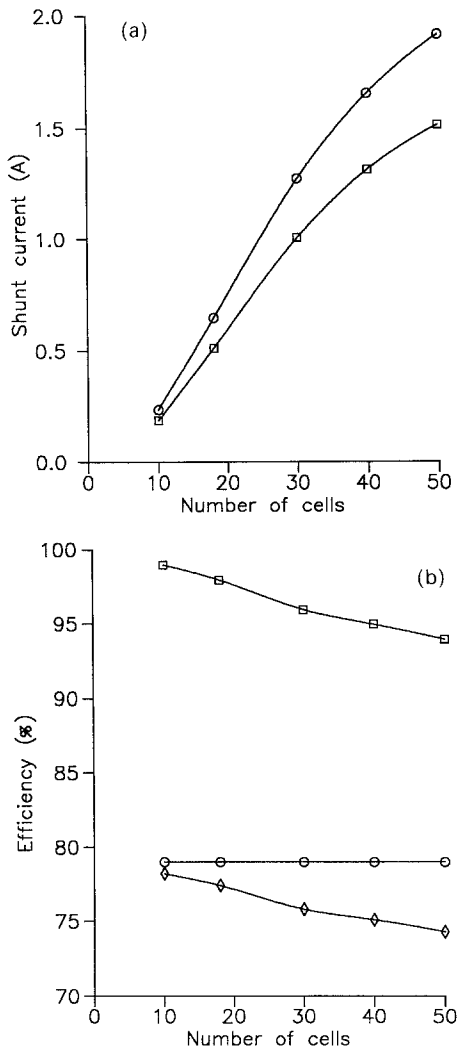

Fig. 3. (a) Representation of the shunt current at the central cell of the stack as a function of the number of cells. (○) Charge, (□) discharge. (b) System efficiencies as a function of the number of cells. (○) Voltage, (□) current and (◇) energy. System: single-stack assembly. Input parameters: $R_M = 1.73\,\Omega$, $R_c = 221\,\Omega$, $R_i = 0.003\,\Omega$, $I_t = 40\,A$, $V_o = 1.032\,V$.

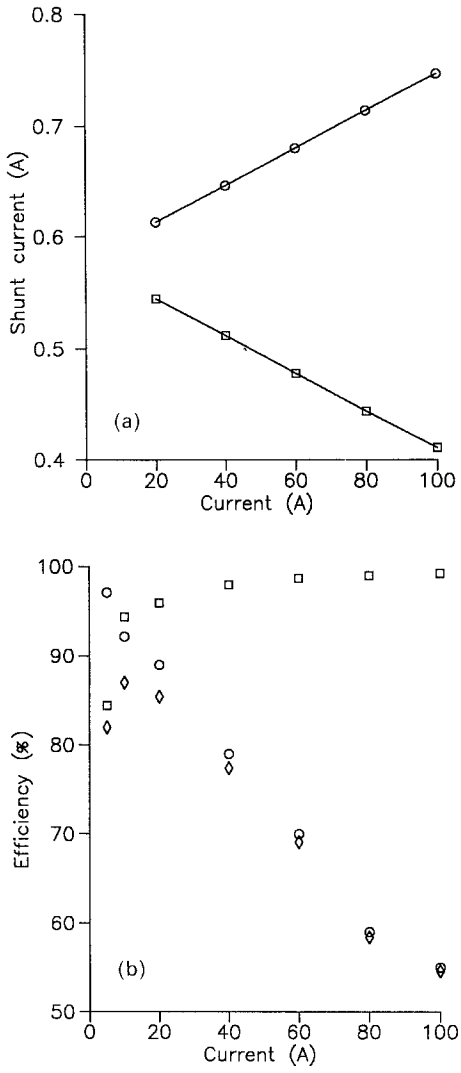

Fig. 4. (a) Representation of the shunt current at the central cell of the stack as a function of charge-discharge current. (○) Charge, (□) discharge. (b) System efficiencies as a function of the charge-discharge current. (○) Voltage, (□) current and (◇) energy. System: single-stack assembly. Input parameters: $R_M = 1.73\,\Omega$, $R_c = 221\,\Omega$, $R_i = 0.003\,\Omega$, $N = 18$ cells, $V_o = 1.032\,V$.

shown as a function of the charge-discharge current. Linear dependence has been found since each cell is considered as an ideal d.c. voltage source and its voltage is a linear function of the current. For the same reason, shunt current decreases when the discharge current is increased. The fact that the absolute values of the slopes are less than one implies that the shunt current/stack current ratio is smaller when the stack current is increased and therefore the current efficiency increases (Fig. 4b).

However, this increase of the stack current provides a predictable decrease of voltage efficiency. As a direct consequence of the inverse behaviour presented by current and voltage efficiencies at an increase in the total current, energy efficiency reaches a maximum at a total current of around 10 A (10 mA cm^{-2}). From these results, it can be concluded that over 75% energy efficiencies can be reached working with total currents up to 40 A. If power demand is increased, the designed system could work at total currents of 60 A with a close to 70% energy efficiency.

3.1.3. Manifold and port cross-section. The influence of manifold and port cross-section on energy efficiency has been studied. Manifold and port length was previously fixed due to the fact that these parameters are related to other design factors such as mechanical stability of flow distribution frames, electrode and gasket thickness, etc. In Fig. 5 energy efficiency as a function of manifold and port cross-section is shown. When the manifold cross-sections are increased, energy efficiency becomes dependent on the port cross-section only. On the contrary, when the port cross-sections are increased, energy efficiency is very dependent on the manifold cross-section.

From these results, one may be expected to operate with a wide range of manifold and port cross-sections with energy efficiency consistently over 70%.

3.2. *Three-stack assembly analysis*

The design parameters of a 2.1 kW three-stack battery are presented in Table 2. The parameters studied were the length of the hydraulic interconnection pipe and

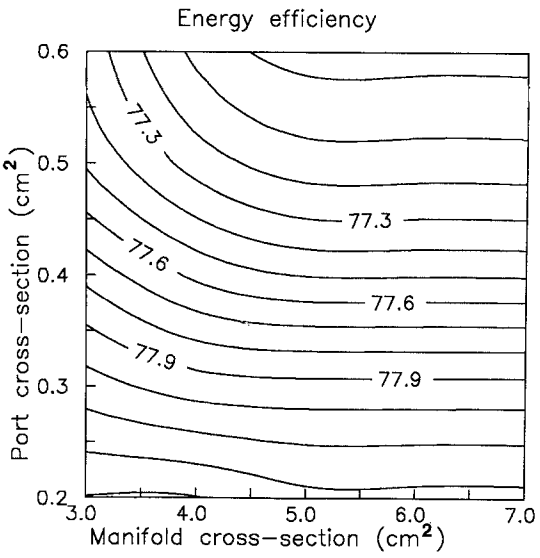

Fig. 5. Level-line diagram corresponding to the system energy efficiency as a function of port and manifold cross-section. System: single-stack assembly. Input parameters: R_i = 0.003 Ω, I_t = 40 A, N = 18 cells, V_0 = 1.032 V.

the total current. Figure 6 shows the shunt current as a function of cell position for charge (Fig. 6a) and similarly for discharge (Fig. 6b). As found for a single stack, shunt currents flow in the opposite direction to the stack current when the battery is in charge. In discharge, shunt currents flow in the same way as the stack current.

However, an enhancement of shunt currents has been found at the central stack in comparison to the terminal ones as a consequence of their connection in series with parallel flow distribution. Logically, this fact has a notable influence on the energy efficiency of the system. Therefore, once the design parameters of a single stack have been fixed, an analysis of the characteristic design parameters of the assembly of stacks (hydraulic interconnection length and total current) must be carried out.

3.2.1. Hydraulic interconnection length. The hydraulic interconnection length was selected as design parameter versus its cross-section, because this last parameter is strongly influenced by other factors of a mechanical nature. In Fig. 7a, shunt current at the central cell of each stack is shown as a function of the interconnection length in charge operation. The calculations were made from a length of 0.5 m as this length is the minimum available if the external size of the stacks is considered.

Table 2. Nominal design specifications for the three-stack redox flow battery

Nominal power	2.1 kW
Gross power	4.8 kW
Voltage (o.c., 50% state of charge)	55.8 V
Number of stacks	3
Number of cells per stack	18
Cell active area	1000 cm²
Nominal current density	40 mA cm^{-2}
Cell resistivity	3 Ω cm²
Equivalent resistors	
Port	221 Ω
Manifold	1.73 Ω
Hydraulic interconnection	20 Ω

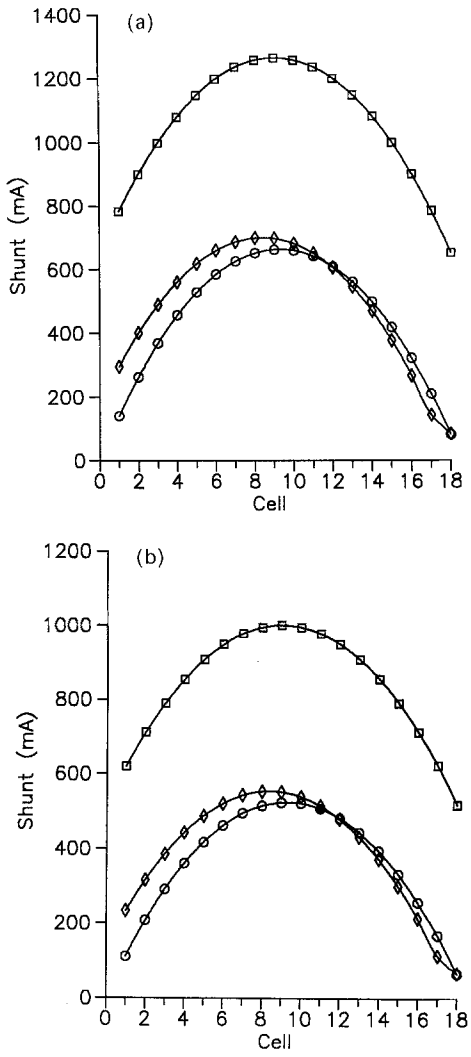

Fig. 6. Representation of shunt current at the central cell of each stack as a function of cell position for (a) charge and (b) discharge. (○) Stack 1, (□) stack 2 and (◇) stack 3. System: three-stack assembly. Input parameters: R_M = 1.73 Ω, R_c = 221 Ω, R_i = 0.003 Ω, R_l = 20 Ω, N = 18 cells, I_t = 40 A, V_0 = 1.032 V.

A great influence of shunt current on the central stack is observed, but it is less significant on the terminal ones. The system has behaved in an identical manner in discharge. However, the calculated shunt currents were lower than those calculated in charge due to the fact that the voltage of each cell is always lower in discharge.

Figure 7b, shows the variation of the system efficiencies as a function of the interconnection length. No significant variations in voltage efficiency are observed because the limiting factor is the internal cell resistance due to the low voltage variations induced by shunt currents compared with the open-circuit cell voltage. It must also be pointed out that the three-stack assembly almost reaches the same current efficiency as the single-stack with the minimum interconnection length tested.

3.2.2. Total current. The influence of the total current on the energy efficiency has been studied. The current

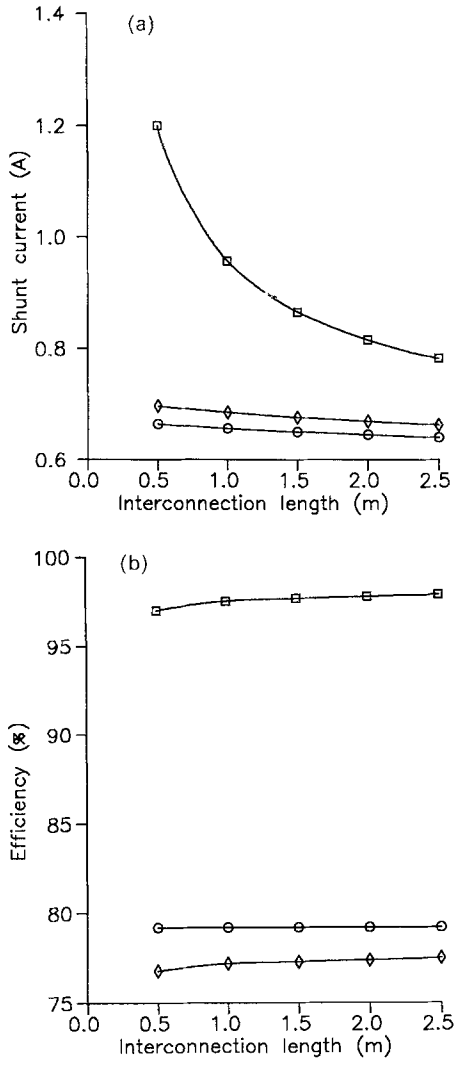

Fig. 7. (a) Representation of shunt current at the central cell of each stack as a function of hydraulic interconnection length in charge operation. (○) Stack 1, (□) stack 2 and (◇) stack 3. (b) System efficiencies as a function of the hydraulic interconnection length. (○) Voltage, (□) current and (◇) energy. System: three-stack assembly. Input parameters: $R_M = 1.73\,\Omega$, $R_c = 221\,\Omega$, $R_i = 0.003$, $N = 18$ cells, $I_t = 40\,A$, $V_0 = 1.032\,V$.

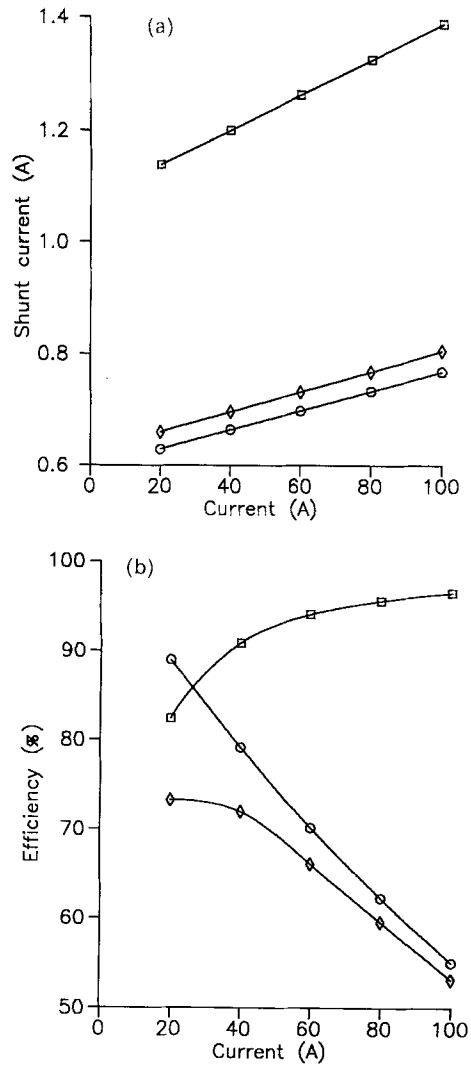

Fig. 8. (a) Representation of shunt current at the central cell of each stack as a function of the charge-discharge current. (○) Stack 1, (□) stack 2 and (◇) stack 3. (b) System efficiencies as a function of the charge-discharge current. (○) Voltage, (□) current and (◇) energy. System: three-stack assembly. Input parameters: $R_M = 1.73\,\Omega$, $R_c = 221\,\Omega$, $R_i = 0.003$, $R_l = 20\,\Omega$, $N = 18$ cells, $V_0 = 1.032\,V$.

and the number of cells of the assembly are the power-fixing parameters of the system. Therefore, it is interesting to analyse the response of the system to several charge-discharge currents. In Fig. 8a shunt current at the central cell of each stack is shown as a function of the charge current. From the shunt current and voltage distribution observed in the previous analysis, a linear increase of the shunt current must be expected with the total current due to the ohmic nature of the voltage variations of the cell.

The decrease in shunt currents observed when the discharge current is increased is due to the same reason. The absolute values of the slopes are less than one and, therefore, when the total current is increased, the shunt current/total current ratio is decreased. Thus, an increase in the current efficiency must be expected when the operation current is increased. However, the diminution of the voltage efficiency as a consequence of the rise in the ohmic drop leads to the fact that energy efficiency reaches a maximum around 20 A. An approximately 75% energy efficiency may be expected when operating at a current of 50 A.

4. Conclusions

A simple method to perform scale-up studies of a redox flow battery based on shunt current analysis has been presented. The application of this model to the design of a 0.7 kW redox flow battery has yielded an over 77% energy efficiency, using the shunt current calculation model presented in the literature [22]. A model for calculating shunt currents in assemblies formed by bipolar stacks connected in series with parallel electrolyte feeding has been developed. The model needs only moderate programming or hardware requirements and it is in good agreement with calculations reported in the literature [22].

From the results herein, the enhancement of shunt currents as a consequence of the connection in series of several bipolar stacks with parallel electrolyte feeding must be pointed out. These shunt currents are significantly more important in the central stack. The

scale-up of the single-stack battery to the three-stack assembly using this model has yielded an energy efficiency similar to that obtained for the single-stack system using a short hydraulic interconnection of the stacks.

Acknowledgement

The authors wish to thank Miguel Angel Pastor and Dr Roberto Duo for their support during these studies. Financial support given by Iberdrola S.A. and Tudor S.A. is also acknowledged.

References

[1] M. Bartolozzi, *J. Power Sources* **27** (1989) 219.
[2] D. Pletcher, in 'Industrial Electrochemistry', (edited by ...) Chapman & Hall, London (1982) p. 88.
[3] K. Kanari, K. Nozaki and T. Ozawa, in 'AIChE Symposium Series, Electrochemical Applications', (edited by R. E. White, R. F. Savinell and A. Schneider), Vol. 83, (1987) p. 104.
[4] P. R. Prokopius, NASA TM X-3359 (1976).
[5] M. A. Hoberecht, DoE/NASA/12726-7, NASA TM-82598 (1981).
[6] D. A. Johnson and M. A. Reid, *J. Electrochem. Soc.* **132** (1985) 1058.
[7] C. Y. Yang, *J. Appl. Electrochem.* **12** (1982) 425.
[8] D. Sh. Cheng and E. Hollax, *J. Electrochem. Soc.* **132** (1985) 269.
[9] C. D. Wu, D. A. Scherson, E. J. Calvo, E. B. Yeager and M. A. Reid, *ibid.* **133** (1986) 2109.
[10] M. Lopez-Atalaya, G. Codina, J. R. Perez, M. A. Climent, J. L. Vazquez and A. Aldaz, *J. Power Sources* **35** (1991) 225.
[11] A. Rodes, A. Aldaz, P. Garces and M. A. Climent, *Bull. Electrochem.* **5** (1989) 129.
[12] G. Codina, M. Lopez-Atalaya, J. L. Vazquez, A. Aldaz and P. Garces, *ibid.* **5** (1989) 645.
[13] D. A. Aikens and J. W. Ross, *J. Phys. Chem.* **65** (1965) 1213.
[14] G. H. Kelsall, C. J. House and F. P. Gudyanga, *J. Electroanal. Chem.* **244** (1988) 179.
[15] R. E. Hamm and C. M. Shull, *J. Am. Chem. Soc.* **73** (1951) 1240.
[16] R. F. Gahn, N. H. Hagedorn and J. A. Johnson, DoE/NASA/121726-25, NASA TM-87034 (1985).
[17] N. Hagedorn, M. A. Hoberecht and L. H. Thaller, DoE/NASA/12726-11. NASA TM-82686 (1986).
[18] E. A. Kaminski and R. F. Savinell, *J. Electrochem. Soc.* **130** (1983) 1103.
[19] P. G. Grimes, R. J. Bellows and M. Zahn, in 'Electrochemical Cell Design', (edited by R. E. White), Plenum, New York (1984) p. 259.
[20] P. Grimes and R. J. Bellows, in *ibid.* p. 277.
[21] J. W. Holmes and R. E. White, in *ibid.* p. 311.
[22] R. E. White, C. W. Walton, H. S. Burney and R. W. Beaver, *J. Electrochem. Soc.* **133** (1986) 485.
[23] S. Szpak, C. J. Gabriel and J. R. Driscoll, *ibid.* **131** (1984) 1996.
[24] M. Katz, *ibid.* **125** (1978) 515.
[25] A. F. Kuhn and J. S. Booth, *J. Appl. Electrochem.* **10** (1980) 233.
[26] H. S. Burney and R. E. White, *J. Electrochem. Soc.* **135** (1988) 1609.
[27] S. Szpak, C. J. Gabriel, J. J. Smith and J. R. Driscoll, *ibid.* **137** (1990) 849.
[28] C. Froberg, in 'Introduction to Numerical Analysis', Adison-Wesley, New York (1969) p. 112.